

# HYDRA: Hybrid Robot Actions for Imitation Learning

Anonymous Author(s)

Affiliation

Address

email

1       **Abstract:** Imitation Learning (IL) is a sample efficient paradigm for robot learn-  
2       ing using expert demonstrations. However, policies learned through IL suffer from  
3       state distribution shift at test time, due to compounding errors in action prediction  
4       which lead to previously unseen states. Choosing an action representation for  
5       the policy that minimizes this distribution shift is critical in imitation learning.  
6       Prior work propose using temporal action abstractions to reduce compounding  
7       errors, but they often sacrifice policy dexterity or require domain-specific knowl-  
8       edge. To address these trade-offs, we introduce HYDRA, a method that leverages  
9       a hybrid action space with two levels of action abstractions: *sparse high-level*  
10      *waypoints* and *dense low-level actions*. HYDRA dynamically switches between  
11      action abstractions at test time to enable both coarse and fine-grained control of  
12      a robot. In addition, HYDRA employs action relabeling to increase the consis-  
13      tency of actions in the dataset, further reducing distribution shift. HYDRA  
14      outperforms prior imitation learning methods by 30-40% on seven challenging  
15      simulation and real world environments, involving long-horizon tasks in the real  
16      world like making coffee and toasting bread. Videos are found on our website:  
17      <https://tinyurl.com/3mc6793z>

## 18   1 Introduction

19   In recent years, supervised learning methods have made remarkable advancements in computer vi-  
20   sion (CV), natural language processing (NLP), and human-level game playing [1, 2, 3, 4, 5, 6, 7].  
21   In robotics, *imitation learning* (IL) has emerged as a data-driven and sample efficient approach for  
22   programming robots using expert demonstrations. More specifically, behavioral cloning (BC) meth-  
23   ods treat IL as a supervised learning problem and directly train a policy to map states to actions. BC  
24   methods are often favored in practice for their simplicity but suffer from the well-known distribu-  
25   tion shift problem, where the test time state distribution deviates from the training state distribution,  
26   primarily caused by the accumulation of errors in action predictions [8, 9, 10].

27   Broadly, prior work has explored reducing distribution shift by interactively adding new data [9],  
28   incorporating large prior datasets [11, 12], choosing better state representations (inputs) [13, 14],  
29   or altering model or loss structure [15, 16, 14]. A less explored but critical factor is the *action*  
30   representation (outputs): action prediction error partially stems from how difficult it is for the policy  
31   to capture the expert demonstrated actions, so action representations are a critical line of defense  
32   against distribution shift. Prior work studying action representations generally fall into two camps:  
33   (1) methods that use *temporal abstractions* to treat long action sequences as a single action (i.e.,  
34   reducing the effective task horizon) and thus reduce the potential for compounding errors, and (2)  
35   methods that make the action representation more *expressive* to minimize the single-step prediction  
36   error [17, 18, 16, 19, 15]. However, both approaches come with a number of shortcomings.

37   Methods using *temporal abstractions* often come at the cost of either the dexterity of the robot  
38   or the generality to new settings. One prior approach is for the robot to follow waypoints that  
39   cover multiple time steps [17, 14]; however, waypoints alone are not reactive enough for dynamic,  
40   dexterous action sequences (e.g., inserting a coffee pod). Other works use structured movement

41 primitives that can capture more dynamic behaviors like skewering food items or helping a person  
42 get dressed [20, 18, 21], but relying on pre-defined primitives often sacrifice generalizability to new  
43 settings (e.g., new primitives beyond skewering for food manipulation). Today, we lack temporal  
44 abstractions that reduce distribution shift without losing policy dexterity and generality.

45 Other methods design each action to be more *expressive* to capture the multi-modality present in  
46 human behavior [19, 15, 16]; however, these expressive action spaces often lead to overfitting, high  
47 training time, or complex learning objectives. Rather than making the policy more expressive, a  
48 more robust approach is to make the actions in the dataset more *consistent* at a given state and easier  
49 to learn (e.g., showing one consistent way to insert a coffee pod rather than many conflicting ways).  
50 Prior work shows that more action consistency (e.g., consistent human demonstrators) with sufficient  
51 state coverage lead to better policies [19, 14, 22], likely by reducing online policy errors [23].

52 To enable both a better temporal abstraction and more consistent actions in the dataset, our key  
53 insight is to leverage the fact that most robotics tasks are hierarchical in nature – they can be divided  
54 into two distinct *modes* of behaviors: *reaching high-level waypoints* (e.g., free-space motion) or  
55 *fine-grained manipulation* (e.g., object interaction). Then, we can learn a policy that dynamically  
56 switches between these modes – this is in fact similar to models of human decision making, where  
57 it is widely believed that humans can discover action abstractions and switch between them during  
58 a task [24, 25]. Capturing both waypoints and fine-grained actions enables us to compress action  
59 sequences (i.e., reduce distribution shift) without sacrificing the dynamic parts of the task, thus  
60 maintaining dexterity. In practice, this abstraction is general enough to represent most tasks in  
61 robot manipulation. Another notable advantage of partitioning tasks into two modes is that, during  
62 the waypoint reaching phase, we can *relabel* our actions with more consistent waypoint-following  
63 behaviors, thus increasing action consistency in the dataset.

64 Leveraging this insight, we propose HYDRA, a method that dynamically switches between two ac-  
65 tion representations: *sparse* waypoint actions for free-space linear motions and *dense*, single-step  
66 delta actions for contact-rich manipulation. HYDRA learns to switch between these action modes  
67 with human-labeled modes, which are provided after or during data collection with minimal ad-  
68 ditional effort. In addition, HYDRA *relabels* low-level actions in the dataset during the waypoint  
69 periods – where the robot is moving in free space (e.g., when reaching a coffee pod) to follow consis-  
70 tent paths. These consistent actions simplify policy learning, which reduces action prediction error  
71 in the dataset overall and thus reduces distribution shift. HYDRA outperforms baseline imitation  
72 learning approaches across seven challenging, long-horizon manipulation tasks spanning both sim-  
73 ulation and the real world. In addition, it is able to perform a complex coffee making task involving  
74 many high precision stages with 80% success, 4x the performance of the best baseline, BC-RNN.

## 75 2 Related Work

76 **Data Curation:** Several prior works aim to *curate* data based on some notion of data quality, in  
77 order to reduce distribution shift. Most works define quality as the state diversity present in a dataset,  
78 To increase state diversity, Ross et al. [9] proposed to interactively collect *on-policy* demonstration  
79 data, but this requires experts to label actions for newly visited states. To reduce expert supervision,  
80 some methods use interventions to relabel on-policy data, where interventions can be automatically  
81 or human generated [26, 27, 28, 29, 22, 30]. Laskey et al. [31] inject noise during data collection  
82 to increase state diversity to achieve similar performance as interactive methods. Recent work has  
83 sought to formalize a broader notion of data quality beyond just state diversity [23]. HYDRA takes  
84 this broader definition into account, increasing data quality through action consistency.

85 **Model and State Priors:** Rather than changing the data, many prior works build in structure to the  
86 model itself to address distribution shift. Object-centric state representations have been shown to  
87 make policies more generalizable [13]. Similarly, pretrained state representations trained on multi-  
88 task data have been shown to improve sample efficiency and robustness [12, 32]. Adding structure  
89 into the model itself, for example using implicit representations or diffusion-based policies, has also  
90 been shown to improve performance [16, 15]. The changes in HYDRA affect the action space and  
91 thus are compatible with many of these prior approaches.

92 **Action Representations:** Another approach is to change the action representation to reduce com-  
 93 pounding errors. One category of prior works leverage *temporal action abstractions* to reduce the  
 94 number of policy steps. Several works have learned skills from demonstrations, usually requiring  
 95 lots of data but struggling to generalize [33, 34, 14]. Others use parameterized action primitives  
 96 or motion primitives, but despite being more sample efficient, these often require privileged state  
 97 information or are not general enough for all scenes [20, 18, 21]. Waypoint action spaces have also  
 98 been shown to be a sample efficient temporal abstraction; however, they fail to capture dynamic and  
 99 dexterous tasks in the environment [35, 16]. For more dexterity, Johns [36] proposes Coarse-to-Fine  
 100 Imitation Learning by modeling a single demonstrated trajectory as two parts: an approaching trajec-  
 101 tory followed by an interaction trajectory. This approach, however, cannot easily scale to multi-step  
 102 manipulation tasks with multiple stages of unstructured object interaction. HYDRA builds on these  
 103 works, combining waypoints and low-level actions into one model to reduce compounding errors  
 104 without losing dexterity or generality. Another category of works seek to increase the *expressiv-*  
 105 *ity* of a single action to reduce action prediction error, for example with Gaussian mixture models  
 106 or energy models [19, 15, 16]. However, increasing expressivity often leads to overfitting, more  
 107 complex learning objectives, and increased training and evaluation time. Instead of increasing ex-  
 108 pressivity, HYDRA takes a more robust approach by increasing action *consistency* in the data. Prior  
 109 work shows the importance of consistent actions for minimizing distribution shift [19, 23]. HYDRA  
 110 relabels actions in the dataset after data collection to increase consistency.

### 111 3 Preliminaries

112 Imitation learning (IL) assumes access to a dataset  $\mathcal{D} = \{\tau_1, \dots, \tau_n\}$  of  $n$  expert demonstra-  
 113 tions. Each demonstration  $\tau_i$  is a sequence of observation-action pairs of length  $N_i$ ,  $\tau_i =$   
 114  $\{(o_1, a_1), \dots, (o_{N_i}, a_{N_i})\}$ , with observations  $o \in \mathcal{O}$  and actions  $a \in \mathcal{A}$ .  $\mathcal{O}$  often consists of robot  
 115 proprioceptive data such as end effector poses and gripper widths, denoted  $s_p \in \mathcal{P}$ , as well as envi-  
 116 ronment observations such as images or object poses, denoted  $s_e \in \mathcal{E}$ , such that  $\mathcal{O} = \mathcal{P} \oplus \mathcal{E}$ . The  
 117 true state of the environment is  $s \in \mathcal{S}$ . In robotics, the action space usually consists of either torque,  
 118 velocity, or position commands for the robot. While velocity actions are most common, prior works  
 119 also use position actions in the form of target waypoints [14, 35]. The IL objective is to learn a  
 120 policy  $\pi_\theta : \mathcal{O} \rightarrow \mathcal{A}$  mapping from observations to actions via the supervised loss:

$$\mathcal{L}(\theta) = -\mathbb{E}_{(o,a) \sim \mathcal{P}_{\mathcal{D}}} [\log \pi_\theta(a|o)] \quad (1)$$

121 At test time, the learned policy  $\pi_\theta$  is rolled out under environment dynamics  $f : \mathcal{S} \times \mathcal{A} \rightarrow \mathcal{S}$ . Per  
 122 step, we observe  $o_t$ , sample an action  $\tilde{a}_t \sim \pi(\cdot|o_t)$ , and obtain the next state  $s_{t+1} = f(s_t, \tilde{a}_t)$ .

123 **Distribution Shift in IL.** A fundamental challenge with imitation learning is state *distribution shift*  
 124 between training and test time. Considering training sample  $(\dots, o_t, a_t, o_{t+1} \dots)$ : if the learned  
 125 policy outputs  $\tilde{a}_t \sim \pi(\cdot|o_t)$ , which has a small action error  $\epsilon_t = \tilde{a}_t - a_t$ , the next state following  
 126 this action will also deviate:  $\tilde{s}_{t+1} = f(s_t, a_t + \epsilon_t)$ , which in turn affects the policy output at the  
 127 next step. For real world dynamics, this change in next state can be highly disproportionate to  $\|\epsilon_t\|$ .  
 128 For example in the coffee task in Fig. 1, with a slight change in gripper position (small  $\epsilon_t$ ) the policy  
 129 can misgrasp the coffee pod (large change in  $s_{t+1}$  and  $o_{t+1}$ ). Furthermore, noise in the dynamics  
 130  $f$  can lead to even larger changes in  $o_{t+1}$ . As we continue to execute for the next  $N - t$  steps, this  
 131 divergence from the training distribution can compound, often leading to task failure.

132 Therefore, reducing distribution shift requires reducing  $\epsilon_t$  for all  $t \in \{1, \dots, N\}$  or increasing the  
 133 coverage of states  $s_t$ . One approach to reduce policy error is increasing **action consistency**, which  
 134 prior work defines as lowering the entropy of the expert policy  $\pi_E$  at each state:  $\mathcal{H}_{\pi_E}(a|s)$  [23].  
 135 However, there is a trade-off between state coverage and action consistency during data collection,  
 136 since less consistent actions often lead to more diverse states [23, 19]. HYDRA reduces distribution  
 137 shift by using a temporal abstraction for the action space – which shortens the number of policy  
 138 steps  $N$  and thus reduces compounding errors – and by improving action consistency in offline data  
 139 – which reduces  $\|\epsilon_t\|$  without reducing state coverage.

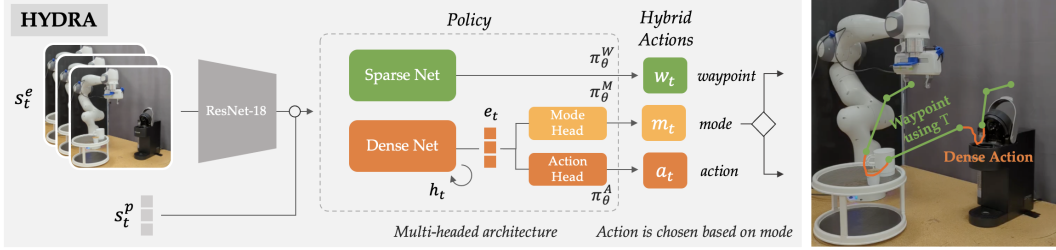


Figure 1: Multi-headed architecture of HYDRA: During training, we learn to predict waypoints, low level actions, and the mode label for each time step. One network (Dense Net) predicts the low level action  $a_t$  and the mode  $m_t$ ; both the action and mode heads of Dense Net share an intermediate representation  $e_t$ . A separate network (Sparse Net) predicts the high level waypoint  $w_t$ . At test time, we sample  $m_t$  and either servo to reach a waypoint ( $m_t = 0$ ) without requering the policy, or follow a dense action for one time step ( $m_t = 1$ ). An example of how sparse and dense modes can be arbitrarily stitched together at test time is shown on the right.

#### 140 4 HYDRA: A Hybrid Action Representation

141 To reduce distribution shift, our insight is that most robot manipulation tasks are a combination of  
 142 *sparse* waypoint-reaching, such as reaching for an object or lifting a mug towards a shelf, and *dense*  
 143 low-level actions, such as grasping an object or balancing a mug stably on a shelf. Waypoints capture  
 144 free-space motions but struggle to capture dexterous or precise behaviors. Conversely, low-level  
 145 actions capture these dynamic behaviors but are often redundant during long free-space motions.

146 Instead of learning from only velocities or waypoints, HYDRA learns a *hybrid action representation*  
 147 consisting of both high-level waypoints in the robot’s proprioceptive space  $w \in \mathcal{P}$  and low-level ac-  
 148 tions  $a \in \mathcal{A}$ . Additionally, we learn to dynamically switch between these modes by predicting which  
 149 mode  $m \in \{0, 1\}$ , sparse or dense, should be executed at each demonstrated state. Mode labels are  
 150 annotated with little extra cost by experts either during or after data collection. This flexible ab-  
 151 straction leads to (1) a compressed action space that reduces compounding errors without sacrificing  
 152 dexterity or generality, and (2) a more consistent, simple low-level action distribution through action  
 153 relabeling during the sparse periods. This section presents an overview of the approach, followed by  
 154 discussions on mode labeling, action relabeling, and training/testing procedures.

155 **Overview:** The multi-headed architecture of HYDRA is outlined in Fig. 1, with heads  $\pi_\theta^M : \mathcal{O} \rightarrow$   
 156  $\{0, 1\}$ ,  $\pi_\theta^A : \mathcal{O} \rightarrow \mathcal{A}$ ,  $\pi_\theta^W : \mathcal{O} \rightarrow \mathcal{P}$ , for mode, action, and waypoint respectively. One network,  
 157 Dense Net, predicts the low-level action  $a_t$  and the mode  $m_t$  at each input  $o_t = \{s_t^e, s_t^p\}$ . Another  
 158 network, Sparse Net, separately outputs the desired *future* waypoint  $w_t$  for input  $o_t$ . We assume  
 159 waypoints can be reached using a known controller  $T : \mathcal{O} \times \mathcal{P} \rightarrow \mathcal{A}$  which converts the state and  
 160 desired waypoint into a low-level action (e.g. a linear controller, see the right side of Fig. 1). In prac-  
 161 tice, Dense Net is recurrent since both the mode and action are highly dependent on history. Sparse  
 162 Net on the other hand only uses the current observation to predict the waypoint, since waypoints are  
 163 less multi-modal and history dependent than actions. Then at test time, HYDRA predicts the mode  
 164  $m_t$  and follows the controller  $T$  until reaching the waypoint during predicted sparse periods, and  
 165 follows low-level actions at each step during predicted dense periods.

##### 166 4.1 Data Processing: Mode Labeling and Action Consistency

167 To dynamically switch action abstractions, we need labeled modes  $m_t$ , waypoints  $w_t$ , and actions  
 168  $a_t$  at each time step. We first obtain binary mode labels  $m_t$  from humans, and then use the mode  
 169 labels to extract waypoints and to relabel low-level actions. Importantly, modes can be labeled either  
 170 online (during demonstration collection, e.g. with a simple button interface), or entirely offline (after  
 171 demonstration collection, e.g., labeling each frame with its mode). With modes labeled, we can  
 172 segment each demonstration into sparse waypoint and dense action phases. We provide the details  
 173 of the labeling and segmentation process in Appendix B. For each sparse phase, we can extract the  
 174 desired future waypoint  $w_t$  at  $o_t$ : if  $m_t = 0$  (sparse), the future waypoint is final proprioceptive  
 175 state  $w_t = p_{t'}$  in that sparse segment, where  $t' > t$ . But if  $m_t = 1$  (dense), the waypoint is the next  
 176 proprioceptive state  $w_t = p_{t+1}$ . This yields a dataset of  $\hat{\mathcal{D}}$  of  $(o, a, w, m)$  tuples. Now the policy  
 177 has full supervision to learn the modes, waypoints, and actions.

178 **Mode Labeling Strategy:** Since waypoints will be reached online with controller T, the main  
 179 requirement for labeling modes is that during sparse phases ( $m_t = 0$ ), the labeled waypoint  $w_t$   
 180 should be reachable via T starting from  $o_t$  (i.e., without collision): for example, if the demonstrator  
 181 starts in free space and labels a waypoint close to coffee K-pod, and if the policy uses a linear P-  
 182 controller as T, then the K-pod waypoint should be reachable from the initial pose in a straight-line  
 183 path. Otherwise, the learned policy might collide when it tries to reach similar waypoints. We do not  
 184 assume access to a collision-avoidance planner as T in this work, but if one has access to a planner  
 185 then T can always reach the desired waypoint, so this reachability requirement can be ignored. Other  
 186 considerations for mode labeling and a discussion of mode sensitivity is provided in [Appendix B](#).  
 187 We specifically show that our method is not overly sensitive to mode labeling strategies outside of  
 188 the collision-free requirement above. Furthermore, we show that mode labels can be learned from  
 189 substantially fewer examples without a major effect on performance [Appendix D.3](#).

190 **Relabeling Low-Level Actions:** As discussed in [Section 3](#), action consistency can improve policy  
 191 performance by simplifying the BC objective in [Eq. \(1\)](#) and thus reducing  $\|\epsilon_t\|$ , provided the data  
 192 has enough state coverage. However, making actions consistent during data collection is challenging  
 193 and can often reduce state coverage [\[22\]](#), so instead HYDRA performs *offline* action relabeling, i.e.,  
 194 after collection. To relabel human actions  $a_t$  during the sparse periods, HYDRA uses waypoint  
 195 controller T to “imagine” a new action at each demonstrated robot state  $s_t^p$  based on the waypoint  
 196  $w_t$ . We lack a consistent relabeling strategy for dense periods, so we leave this to future work.

197 However, a subtle challenge with offline relabeling is that changing the actions in the data can put the  
 198 policy out of distribution at test time, since new actions can lead to new states online. For example,  
 199 if an arc path was demonstrated to get to a waypoint, but a linear controller is used for relabeling, the  
 200 linear action will take us off that path. HYDRA avoids this problem by using a waypoint controller  
 201 T online during sparse periods, meaning relabeled actions will not be deployed online. Rather, this  
 202 action relabeling serves primarily to simplify the dense action learning objective of HYDRA and  
 203 increase action consistency in the overall dataset.

204 A natural question arises: since sparse actions will be executed with T online, could we instead  
 205 further simplify learning by avoiding training on dense actions during sparse periods? If HYDRA  
 206 mispredicts a sparse mode as dense, then the dense actions will still be executed online, so HYDRA  
 207 should still be trained on dense actions during sparse periods as a back-up. We show that reducing  
 208 the training weight of dense actions during sparse periods hurts performance in [Appendix D.5](#).

## 209 4.2 Training and Evaluation

210 **Training:** HYDRA is trained to both imitate low-level actions  $a$  with policy  $\pi_\theta^A$ , high-level way-  
 211 points  $w$  with  $\pi_\theta^W$ , and the mode  $m$  with  $\pi_\theta^M$  at each time step. To balance the waypoint and action  
 212 losses, we use a mode-specific loss at each time step that weighs the current mode’s loss with  $(1-\gamma)$ ,  
 213 and the other mode’s loss with  $\gamma$ . Given a processed dataset  $\hat{\mathcal{D}}$  consisting of tuples of  $(o, a, w, m)$ ,  
 214 we modify the loss in [Eq. \(1\)](#) with the new heads of HYDRA (mode, action, and waypoint):

$$\mathcal{L}_a(\theta) = -\mathbb{E}_{(o,a,w,m) \sim p_{\hat{\mathcal{D}}}} [(1 - \alpha_m) \log \pi_\theta^A(a|o) + \alpha_m \log \pi_\theta^W(w|o)] \quad (2)$$

$$\mathcal{L}_m(\theta) = -\mathbb{E}_{(o,a,w,m) \sim p_{\hat{\mathcal{D}}}} [m \log \pi_\theta^M(m = 1|o) + (1 - m) \log \pi_\theta^M(m = 0|o)] \quad (3)$$

215  $\mathcal{L}_a$  weighs the BC loss for waypoints and actions by the current mode:  $\alpha_m = m\gamma + (1 - m)(1 - \gamma)$   
 216 is the mode-specific weight for the sparse waypoint part of  $\mathcal{L}_a$ . If we are in sparse mode ( $m = 0$ ),  
 217 then  $\alpha_m = 1 - \gamma$ , but in dense mode,  $\alpha_m = \gamma$ . Thus, a low gamma encourages the model to fit the  
 218 loss for the current mode *more* than the loss for the other mode, and  $\gamma = 0.5$  will be a mode-agnostic  
 219 weighting. See [Appendix D.5](#) for results of ablating  $\gamma$ .  $\mathcal{L}_m$  is the mode cross entropy classification  
 220 loss. Combining these terms with mode loss weight  $\beta$ , we get the full HYDRA objective:

$$\mathcal{L}(\theta) = \mathcal{L}_a(\theta) + \beta \mathcal{L}_m(\theta) \quad (4)$$

221 **Evaluation:** During evaluation, the policy chooses the mode using  $\tilde{m}_t$ . If  $\tilde{m}_t = 0$ , the model will  
 222 servo in a closed-loop fashion to the predicted waypoint  $\tilde{w}_t$  using controller T. The policy is queried  
 223 at every step to continually update the policy hidden state, but importantly its outputs are ignored  
 224 until we reach the waypoint to avoid action prediction errors. If  $\tilde{m}_t = 1$ , the model will execute just  
 225 the next step using the predicted dense action  $\tilde{a}_t$ .

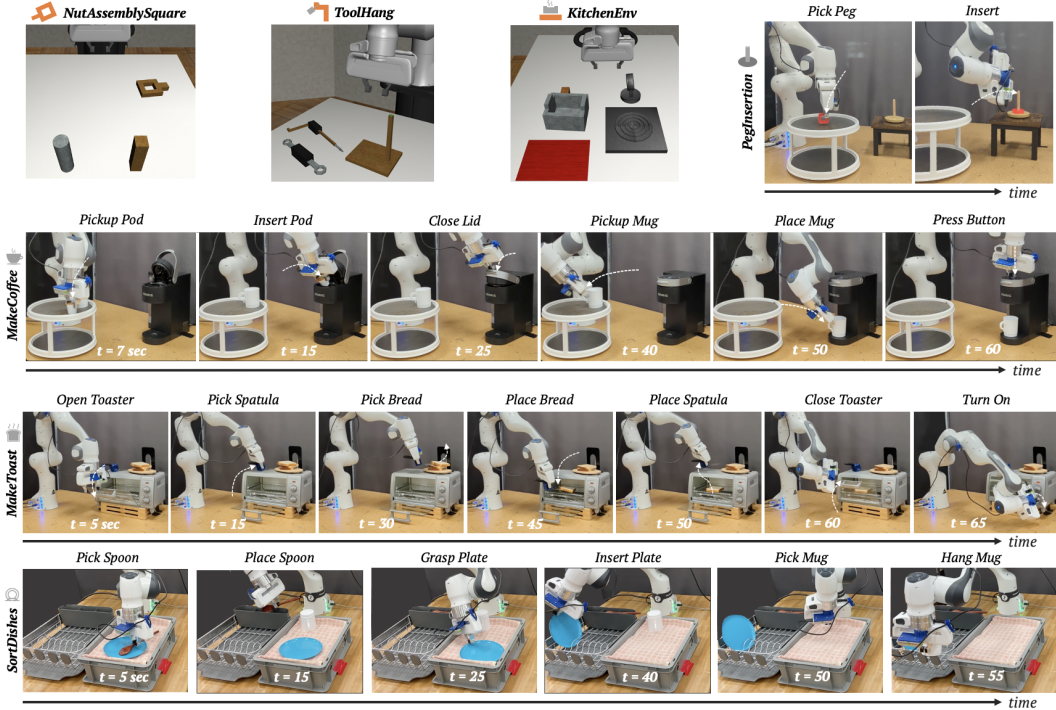


Figure 2: Simulation & Real-world environments, with task stages shown for real world tasks. **Simulation:** In *NutAssemblySquare*, the task is to pick up a square nut at various positions and orientations and insert it onto a vertical square peg. In *ToolHang*, a hanging frame is inserted onto a fixed stand, followed by placing a tool on the frame. Both the frame and tool poses are randomized. Frame insertion is challenging due to the small insertion area. *KitchenEnv* involves turning on a stove, moving a pot onto the stove, putting an object in the pot, then moving the pot to a serving area. **Real World:** *PegInsertion* involves inserting a peg with a hole in the center onto a round insertion rod (top right); the peg location and geometry are varied. *MakeCoffee* is a 6-step task (top middle row) involving picking up a K-pod, inserting it into a Keurig machine, closing the lid of the Keurig, positioning a mug, and then pressing start on the Keurig; the K-pod location and mug orientations are varied. This is a more challenging version of the task used in prior work [13], which did not include the mug component. *MakeToast* has 7-steps (bottom middle row): a hinged toaster oven is opened, a spatula is picked up, bread is placed inside the toaster, the toaster is closed, and the timer dial is turned to start. Both bread and spatula initial poses vary. *SortDishes* (bottom row) has 6 stages: pick up spoon, place spoon in rack, grasp plate and insert it into rack, and grasp mug and hang the mug. All objects vary in initial pose.

## 226 5 Experiments

227 We evaluate the performance of HYDRA in 3 challenging simulation environments and 4 com-  
 228 plex real world tasks, shown in Fig. 2. These tasks cover a wide range of affordances and levels  
 229 of precision, from precisely inserting a coffee pod to picking up bread with a spatula. See Ap-  
 230 pendix C for model hyperparameters, data collection, and training details. In Appendix D, we show  
 231 a waypoint-only baseline, mode labeling strategy ablations, and a relabeling-only ablation where  
 232 action consistency is improved but the waypoint controller is not used online. In Appendix D.3,  
 233 we show that mode labels can be learned with fewer examples without a large drop in performance  
 234 (e.g., using 25% of mode labels drops performance by 10%). Videos can be found on our website:  
 235 <https://tinyurl.com/3mc6793z>.

236 **Data Collection:** We leverage proficient human demonstration data for simulated tasks from  
 237 robomimic [19]. Mode labels and waypoints were annotated offline for simulation datasets as de-  
 238 scribed in Appendix B. Demonstrations for real world tasks were collected by a proficient user using  
 239 VR teleoperation using an Oculus Quest 2. Mode labels and waypoints were provided during data  
 240 collection (online) using the side button on the Quest VR controller with no added collection time.

241 **Simulation:** In Fig. 3 (top row), we compare our method to BC and BC-RNN for the *NutAssem-*  
 242 *blySquare* and *ToolHang* tasks (state-based), as well as the *KitchenEnv* task (vision-based) from  
 243 robosuite (see top row in Fig. 2). Our method improves performance on the *NutAssemblySquare*

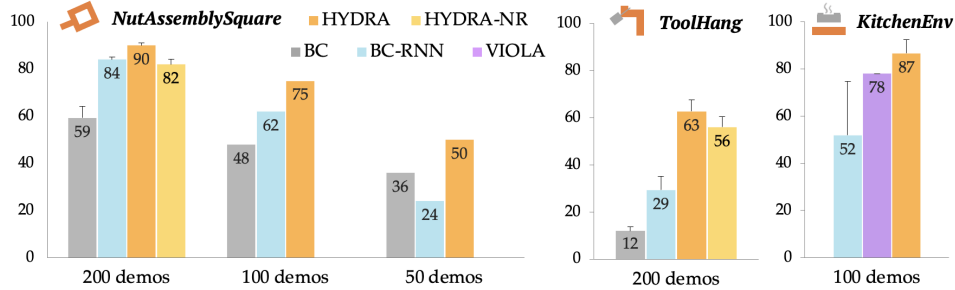


Figure 3: Sim Results for HYDRA vs. BC, BC-RNN, and VIOLA: best checkpoint success rate averaged over three seeds. **Left to Right:** *NutAssemblySquare* (state), *ToolHang* (state), and *KitchenEnv* (vision) tasks. HYDRA beats baselines on all of these tasks, and even beats VIOLA [13] on the kitchen task despite using a much smaller and simpler model. We also show a comparison for BC-RNN and HYDRA with decreasing data sizes for *NutAssemblySquare*, showing that our method is more sample efficient than BC-RNN. HYDRA without action relabeling (HYDRA-NR, *NutAssemblySquare* and *ToolHang*) drops performance by 7-8%.

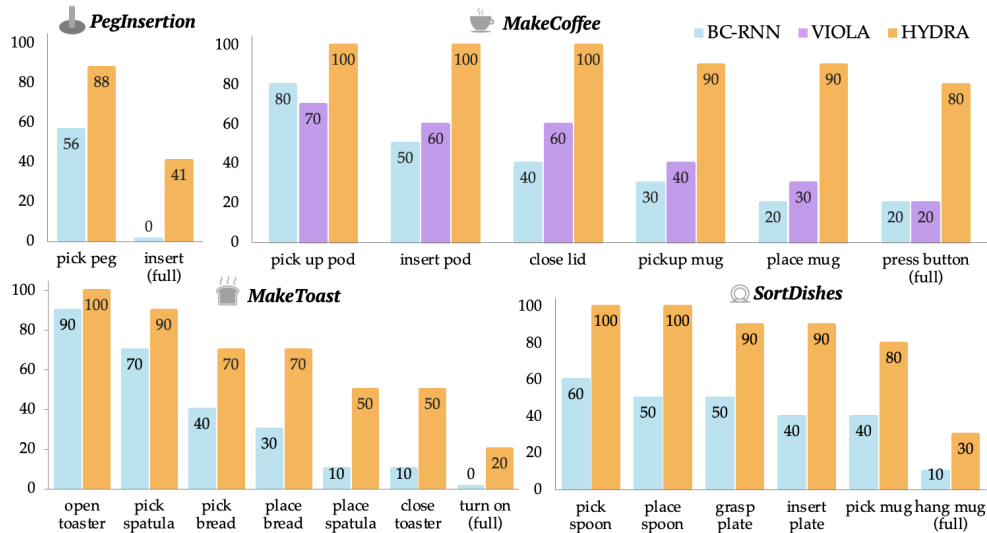


Figure 4: Real Results for HYDRA vs. BC, BC-RNN, and VIOLA. The x-axis denotes each stage (right-most value is the final success rate). **Top Left:** HYDRA vs. BC-RNN on the real *PegInsertion* task for 50 demos under 32 rollouts across 4 different nuts. This task requires very precise grasping and insertion of multiple types of nuts, which our method does with high success. While baseline is unable to perform insertion, HYDRA gets 41% success. **Top Right:** *MakeCoffee* long-horizon task for 100 demos under 10 rollouts. Our method beats baseline by 60%. **Bottom Left:** *MakeToast* long-horizon task for 100 demos under 10 rollouts. While both methods struggle to turn the toaster on, HYDRA is able to reach 50% success for 6/7 stages compared to 10% for baseline. **Bottom Right:** *SortDishes* for 100 demos under 10 rollouts. Waypoints in HYDRA precisely capture the diverse poses in this task, beating BC-RNN by 40% and 20% for the last two stages.

244 task, where baselines are already quite strong. We also ablate the data size from 200 demos to 100  
 245 and 50 in Fig. 3, illustrating that HYDRA is more sample efficient than baselines, with the gap grow-  
 246 ing as data size decreases. HYDRA-NR in Fig. 3 removes action relabeling and drops performance  
 247 by 8%, which we attribute to high action multi-modality in non-relabeled sparse periods.

248 For the *Tool Hang* task (top middle in Fig. 3), which is long horizon and consists of many waypoint  
 249 and dense periods and requiring much higher precision, our method has an even bigger gap in per-  
 250 formance with BC and BC-RNN. While the best baseline gets 29%, our method reaches 63% with  
 251 the same inputs. Once again, removing action relabeling (HYDRA-NR) drops performance by 7%  
 252 but is still substantially better than baseline.

253 For *KitchenEnv* (vision-based), we also compare to VIOLA [13], an image-based model that uses  
 254 bounding box features and a large transformer architecture to predict actions. Once again, HYDRA  
 255 is able to outperform BC-RNN by 35% on this long horizon task. HYDRA also outperforms VIOLA  
 256 by 9%, despite using a simpler and smaller model.

257 **Real World:** In Fig. 4, we compare our method to BC-RNN (vision-based) for four high precision  
258 tasks: *PegInsertion*, *MakeCoffee*, *MakeToast*, and *SortDishes*. The latter three are long-horizon,  
259 and Fig. 4 shows cumulative success per task stage. In *Peg Insertion*, our method substantially  
260 outperforms BC-RNN at both peg grasping and precise insertion portions of the task, thanks to  
261 combining precise waypoints with flexible low level actions where necessary.

262 For *MakeCoffee*, HYDRA once again beats BC-RNN and VIOLA by a substantial margin at all  
263 stages of the task. Although all methods perform well in grasping the K-pod, the performance of  
264 the baselines declines rapidly in the following phases. While BC-RNN failed to do this task in prior  
265 work, we see that with a bit of parameter tuning, BC-RNN is a strong baseline, achieving 20%  
266 performance [13]. The reported performance of VIOLA in prior work for coffee pod insertion and  
267 closing the lid is 60%, which matches with the performance we observe for the corresponding stage  
268 of our coffee task. Our task adds two more stages (picking up and placing a mug before pressing the  
269 button), interestingly causing the final success rate of VIOLA to drop to 20%, the same as BC-RNN.  
270 Using the same parameters and model size as BC-RNN, HYDRA achieves 80% final success at this  
271 task with the same underlying dataset.

272 For *MakeToast* and *SortDishes*, HYDRA performs better on all stages of the task as compared to  
273 BC-RNN. We omit VIOLA in these tasks since, as seen in the coffee task, BC-RNN is a competitive  
274 baseline. Both tasks consists of several bottleneck stages where performance drops sharply. In  
275 *MakeToast*, for picking up bread, the spatula must slide underneath a bread slice – HYDRA passes  
276 this stage 70% of the time, beating BC-RNN by 30%. The last stage (turning the toaster on) is  
277 particularly challenging for all methods, but HYDRA completes it 20% of the time compared to  
278 0% for BC-RNN. In *SortDishes*, the final hang-mug stage similarly requires high precision with  
279 randomized objects. Not including the challenging last stage, HYDRA beats BC-RNN by 40% on  
280 this task. See Appendix D.1 for rollouts of each task for each model.

281 We observe that the performance gain for HYDRA in our real world experiments is notably higher  
282 than in simulation. We hypothesize this is due to (1) higher variance in action playback on the  
283 real robot setup, which HYDRA mitigates during sparse periods using the closed-loop waypoint  
284 controller, and (2) increased potential for compounding errors in longer tasks. Overall, HYDRA is  
285 well-suited to long horizon tasks even with many high-precision bottleneck stages, due to its ability  
286 to switch between waypoints and dense actions and its ability to increase action consistency offline.  
287 We also observed that in our real world tasks, HYDRA exhibits emergent retrying behavior, often  
288 re-servoing to a consistent and in-distribution waypoint to retry a failed dense period.

## 289 6 Discussion

290 **Summary:** In this work, we propose HYDRA, which uses a flexible action abstraction to reduce  
291 compounding errors, and improves action consistency while maintaining the state diversity present  
292 in uncurated human demonstrations. HYDRA learns to dynamically switch between following way-  
293 points and taking low level actions with a small amount of added mode label supervision that can be  
294 provided either online or offline. HYDRA substantially outperforms baselines on three simulation  
295 tasks and four real world tasks that involve long horizon manipulation with many bottleneck states.

296 **Limitations & Future Work:** While only a minor amount of added supervision, HYDRA relies on  
297 having expert-collected mode labels. We show that mode labels can be learned from much less data  
298 in Appendix D.3, but future work might consider using unsupervised methods for mode labeling,  
299 e.g., skill segmentation [37] or automatically extracting “linear” portions of a demonstration. We  
300 also hypothesize multi-task datasets can help learn a general mode-predictor that can be fine-tuned  
301 or deployed zero-shot on novel tasks. Furthermore, when mode labels are collected online, mode  
302 labeling can add a mental load for the demonstrator and might also influence the quality of the data  
303 on its own. Future work might conduct more extensive user studies to better understand the effect  
304 of providing mode labels for both the demonstrator and the final learning performance.

305 Despite these limitations, HYDRA is a simple and easy-to-implement method, and it is exciting that  
306 it shows substantial improvement over state-of-the-art imitation learning techniques and significant  
307 promise in solving challenging manipulation tasks in the real world.

## References

- [1] A. Dosovitskiy, L. Beyer, A. Kolesnikov, D. Weissenborn, X. Zhai, T. Unterthiner, M. Dehghani, M. Minderer, G. Heigold, S. Gelly, et al. An image is worth 16x16 words: Transformers for image recognition at scale. In *International Conference on Learning Representations*, 2020.
- [2] K. He, X. Chen, S. Xie, Y. Li, P. Dollár, and R. Girshick. Masked autoencoders are scalable vision learners. In *Proceedings of the IEEE/CVF Conference on Computer Vision and Pattern Recognition*, pages 16000–16009, 2022.
- [3] A. Radford, J. W. Kim, C. Hallacy, A. Ramesh, G. Goh, S. Agarwal, G. Sastry, A. Askell, P. Mishkin, J. Clark, et al. Learning transferable visual models from natural language supervision. In *International conference on machine learning*, pages 8748–8763. PMLR, 2021.
- [4] T. Brown, B. Mann, N. Ryder, M. Subbiah, J. D. Kaplan, P. Dhariwal, A. Neelakantan, P. Shyam, G. Sastry, A. Askell, et al. Language models are few-shot learners. *Advances in neural information processing systems*, 33:1877–1901, 2020.
- [5] R. Thoppilan, D. De Freitas, J. Hall, N. Shazeer, A. Kulshreshtha, H.-T. Cheng, A. Jin, T. Bos, L. Baker, Y. Du, et al. Lamda: Language models for dialog applications. *arXiv preprint arXiv:2201.08239*, 2022.
- [6] A. Chowdhery, S. Narang, J. Devlin, M. Bosma, G. Mishra, A. Roberts, P. Barham, H. W. Chung, C. Sutton, S. Gehrmann, et al. Palm: Scaling language modeling with pathways. *arXiv preprint arXiv:2204.02311*, 2022.
- [7] S. Reed, K. Zolna, E. Parisotto, S. G. Colmenarejo, A. Novikov, G. Barth-Maron, M. Gimenez, Y. Sulsky, J. Kay, J. T. Springenberg, et al. A generalist agent. *arXiv preprint arXiv:2205.06175*, 2022.
- [8] S. Ross and D. Bagnell. Efficient reductions for imitation learning. In *Proceedings of the thirteenth international conference on artificial intelligence and statistics*, pages 661–668. JMLR Workshop and Conference Proceedings, 2010.
- [9] S. Ross, G. Gordon, and D. Bagnell. A reduction of imitation learning and structured prediction to no-regret online learning. In *Proceedings of the fourteenth international conference on artificial intelligence and statistics*, pages 627–635. JMLR Workshop and Conference Proceedings, 2011.
- [10] J. Spencer, S. Choudhury, A. Venkatraman, B. Ziebart, and J. A. Bagnell. Feedback in imitation learning: The three regimes of covariate shift. *arXiv preprint arXiv:2102.02872*, 2021.
- [11] D. Driess, F. Xia, M. S. M. Sajjadi, C. Lynch, A. Chowdhery, B. Ichter, A. Wahid, J. Tompson, Q. Vuong, T. Yu, W. Huang, Y. Chebotar, P. Sermanet, D. Duckworth, S. Levine, V. Vanhoucke, K. Hausman, M. Toussaint, K. Greff, A. Zeng, I. Mordatch, and P. Florence. Palm-e: An embodied multimodal language model. In *arXiv preprint arXiv:2303.03378*, 2023.
- [12] S. Karamcheti, S. Nair, A. S. Chen, T. Kollar, C. Finn, D. Sadigh, and P. Liang. Language-driven representation learning for robotics. 2023.
- [13] Y. Zhu, A. Joshi, P. Stone, and Y. Zhu. Viola: Imitation learning for vision-based manipulation with object proposal priors. *6th Annual Conference on Robot Learning (CoRL)*, 2022.
- [14] S. Belkhale and D. Sadigh. Plato: Predicting latent affordances through object-centric play. In *6th Annual Conference on Robot Learning*, 2022.
- [15] P. Florence, C. Lynch, A. Zeng, O. A. Ramirez, A. Wahid, L. Downs, A. Wong, J. Lee, I. Mordatch, and J. Tompson. Implicit behavioral cloning. In *Conference on Robot Learning*, pages 158–168. PMLR, 2022.

- 353 [16] C. Chi, S. Feng, Y. Du, Z. Xu, E. Cousineau, B. Burchfiel, and S. Song. Diffusion policy:  
354 Visuomotor policy learning via action diffusion. *arXiv preprint arXiv:2303.04137*, 2023.
- 355 [17] M. Shridhar, L. Manuelli, and D. Fox. Perceiver-actor: A multi-task transformer for robotic  
356 manipulation. In *6th Annual Conference on Robot Learning*, 2022.
- 357 [18] R. P. Joshi, N. Koganti, and T. Shibata. A framework for robotic clothing assistance by imita-  
358 tion learning. *Advanced Robotics*, 33(22):1156–1174, 2019.
- 359 [19] A. Mandlekar, D. Xu, J. Wong, S. Nasiriany, C. Wang, R. Kulkarni, L. Fei-Fei, S. Savarese,  
360 Y. Zhu, and R. Martín-Martín. What matters in learning from offline human demonstrations  
361 for robot manipulation. *arXiv preprint arXiv:2108.03298*, 2021.
- 362 [20] P. Sundaresan, S. Belkhale, and D. Sadigh. Learning visuo-haptic skewering strategies for  
363 robot-assisted feeding. In *6th Annual Conference on Robot Learning*, 2022. URL <https://openreview.net/forum?id=1Lq09gVoaTE>.
- 365 [21] J. Silvério, Y. Huang, F. J. Abu-Dakka, L. Rozo, and D. G. Caldwell. Uncertainty-aware  
366 imitation learning using kernelized movement primitives. In *2019 IEEE/RSJ International  
367 Conference on Intelligent Robots and Systems (IROS)*, pages 90–97. IEEE, 2019.
- 368 [22] K. Gandhi, S. Karamcheti, M. Liao, and D. Sadigh. Eliciting compatible demonstrations for  
369 multi-human imitation learning. In *Proceedings of the 6th Conference on Robot Learning  
370 (CoRL)*, 2022.
- 371 [23] S. Belkhale, Y. Cui, and D. Sadigh. Data quality in imitation learning, 2023.
- 372 [24] L. L. Richmond and J. M. Zacks. Constructing experience: Event models from perception to  
373 action. *Trends in Cognitive Sciences*, 21(12):962–980, 2017. ISSN 1364-6613. doi:<https://doi.org/10.1016/j.tics.2017.08.005>. URL <https://www.sciencedirect.com/science/article/pii/S1364661317301857>.
- 376 [25] C. Baldassano, J. Chen, A. Zadbood, J. Pillow, U. Hasson, and K. Norman. Discovering event  
377 structure in continuous narrative perception and memory, 2016.
- 378 [26] Y. Cui, D. Isele, S. Niekum, and K. Fujimura. Uncertainty-aware data aggregation for deep  
379 imitation learning. In *2019 International Conference on Robotics and Automation (ICRA)*,  
380 pages 761–767. IEEE, 2019.
- 381 [27] R. Hoque, A. Balakrishna, E. Novoseller, A. Wilcox, D. S. Brown, and K. Goldberg.  
382 Thriftydagger: Budget-aware novelty and risk gating for interactive imitation learning. In  
383 *Conference on Robot Learning*, pages 598–608. PMLR, 2022.
- 384 [28] M. Kelly, C. Sidrane, K. Driggs-Campbell, and M. J. Kochenderfer. Hg-dagger: Interactive  
385 imitation learning with human experts. In *2019 International Conference on Robotics and  
386 Automation (ICRA)*, pages 8077–8083. IEEE, 2019.
- 387 [29] A. Mandlekar, D. Xu, R. Martín-Martín, Y. Zhu, L. Fei-Fei, and S. Savarese. Human-in-the-  
388 loop imitation learning using remote teleoperation. *arXiv preprint arXiv:2012.06733*, 2020.
- 389 [30] M. L. Schrum, E. Hedlund-Botti, N. Moorman, and M. C. Gombolay. Mind meld: Personal-  
390 ized meta-learning for robot-centric imitation learning. In *2022 17th ACM/IEEE International  
391 Conference on Human-Robot Interaction (HRI)*, pages 157–165. IEEE, 2022.
- 392 [31] M. Laskey, J. Lee, R. Fox, A. Dragan, and K. Goldberg. Dart: Noise injection for robust  
393 imitation learning. In *Conference on robot learning*, pages 143–156. PMLR, 2017.
- 394 [32] S. Nair, A. Rajeswaran, V. Kumar, C. Finn, and A. Gupta. R3m: A universal visual repre-  
395 sentation for robot manipulation. In *6th Annual Conference on Robot Learning*, 2022. URL  
396 <https://openreview.net/forum?id=tGbpz6yOrI>.

- 397 [33] K. Pertsch, Y. Lee, and J. J. Lim. Accelerating reinforcement learning with learned skill priors.  
398 In *Conference on Robot Learning (CoRL)*, 2020.
- 399 [34] C. Lynch, M. Khansari, T. Xiao, V. Kumar, J. Tompson, S. Levine, and P. Sermanet. Learning  
400 latent plans from play. In *Conference on robot learning*, pages 1113–1132. PMLR, 2020.
- 401 [35] M. Shridhar, L. Manuelli, and D. Fox. Perceiver-actor: A multi-task transformer for robotic  
402 manipulation. In *6th Annual Conference on Robot Learning*, 2022. URL [https://openre  
403 view.net/forum?id=PS\\_eCS\\_WCvD](https://openreview.net/forum?id=PS_eCS_WCvD).
- 404 [36] E. Johns. Coarse-to-fine imitation learning: Robot manipulation from a single demonstration.  
405 In *2021 IEEE international conference on robotics and automation (ICRA)*, pages 4613–4619.  
406 IEEE, 2021.
- 407 [37] T. Kipf, Y. Li, H. Dai, V. Zambaldi, A. Sanchez-Gonzalez, E. Grefenstette, P. Kohli, and  
408 P. Battaglia. CompILE: Compositional imitation learning and execution. In K. Chaudhuri  
409 and R. Salakhutdinov, editors, *Proceedings of the 36th International Conference on Ma-  
410 chine Learning*, volume 97 of *Proceedings of Machine Learning Research*, pages 3418–3428.  
411 PMLR, 09–15 Jun 2019. URL [https://proceedings.mlr.press/v97/kipf19a.  
412 html](https://proceedings.mlr.press/v97/kipf19a.html).
- 413 [38] M. Andrychowicz, F. Wolski, A. Ray, J. Schneider, R. Fong, P. Welinder, B. McGrew, J. To-  
414 bin, O. Pieter Abbeel, and W. Zaremba. Hindsight experience replay. *Advances in neural  
415 information processing systems*, 30, 2017.
- 416 [39] L. Zhang and B. C. Stadie. Understanding hindsight goal relabeling requires rethinking diver-  
417 gence minimization. In *Deep Reinforcement Learning Workshop NeurIPS 2022*.

418 We provide a broader discussion of our method in this appendix. In [Appendix A](#) we list a set of  
419 *motivating* questions that may arise during reading the main text of this work and provide our re-  
420 sponse with links to additional details in corresponding sections in the Appendix. In [Appendix B](#) we  
421 discuss how to collect mode labels, and considerations for how to define waypoint and dense seg-  
422 ments. In [Appendix C](#), we outline training procedures, model architectures, and hyperparameters.  
423 In [Appendix D](#), we provide ablation experiments for our method, including sensitivity to mode la-  
424 bels, learning mode labels from less data, ablations to  $\gamma$ , and robustness of HYDRA to added system  
425 noise.

## 426 A Motivating Questions

427 **Intuitively, why does HYDRA help improve BC?** Humans demonstrate manipulation tasks at an  
428 abstraction level that is different from how the robot interprets the data. A BC agent interprets the  
429 data *literally* as taking a specific action at an exact state while the human is *noisely* reaching for an  
430 object. At the high level, HYDRA improves BC by realigning the task abstraction of the robot to  
431 the human demonstrator during waypoint mode of the task. Concretely, HYDRA curates the dataset  
432 in a way that improves action consistency and optimality without reducing state diversity and hence  
433 allowing the learned policy to stay closer in distribution at test time.

434 **What’s the relationship of HYDRA with works in hindsight relabeling?** Hindsight relabel-  
435 ing [38] is the idea of relabeling past experiences of goal-reaching trajectories with the final state it  
436 reaches to reuse any sub-optimal data (especially for reinforcement learning settings). Recent work  
437 of Zhang and Stadie [39] draws the connection between goal-conditioned imitation learning and  
438 hindsight relabeling from a divergence-minimization perspective. The current implementation of  
439 HYDRA operates in single-task imitation learning setting, and therefore is only remotely related to  
440 the idea in hindsight relabeling. From this perspective, one can think of HYDRA as effectively re-  
441 ducing divergence of the dataset’s action distribution by relabeling actions for the waypoint periods  
442 of the trajectory.

443 **Does online mode labeling change demonstrator behavior?** We explain the online mode labeling  
444 process in [Appendix B](#). We acknowledge that asking the demonstrator to provide online mode label-  
445 ing adds additional cognitive load during demonstrating the task, and at the same time may change  
446 their demonstration behavior. In practice, asking the demonstrator to provide the two mode labels  
447 can communicate the structure the robot leverages to learn tasks and may in turn allow the human  
448 to provide better demonstrations (such as consistent waypoints etc.). However, we leave this user  
449 study to future work.

450 **How sensitive is HYDRA to mode labeling?** In our experiments, we (experts in this task) provided  
451 the mode labels for different tasks. We found HYDRA to be robust to the labeling strategies across  
452 the two labelers. For simulated environments, we use existing datasets and labeled the modes using  
453 an interface that shows the robot view of the task and the human annotator marks whether a frame is  
454 waypoint or dense mode. For real robot tasks, the human demonstrator provides the mode labels as  
455 they provide the demonstration using a button on the teleoperation controller. We provide guidelines  
456 for how to perform mode labeling in [Appendix B](#).

## 457 B Labeling Modes in HYDRA

### 458 B.1 Providing Mode Labels

459 The primary assumption made in HYDRA is the availability of mode labels for sparse and dense  
460 periods. Here we provide a discussion of how mode labels can be collected via a simple binary  
461 “click” interface, either online (during demonstration collection) or offline (after collection). In  
462 either case, we can label dense periods and exact waypoints using a single binary “click” variable  
463 via an external button: to label a waypoint at the end of a sparse period, we provide a single click  
464 at the waypoint state; to label a dense period, we sustain the click until the end of the dense period  
465 (see left image in [Fig. 5](#)). Once clicks are labeled, we demarcate periods in between clicks as sparse  
466 modes, and periods with sustained clicks as dense modes (see right image in [Fig. 5](#)).

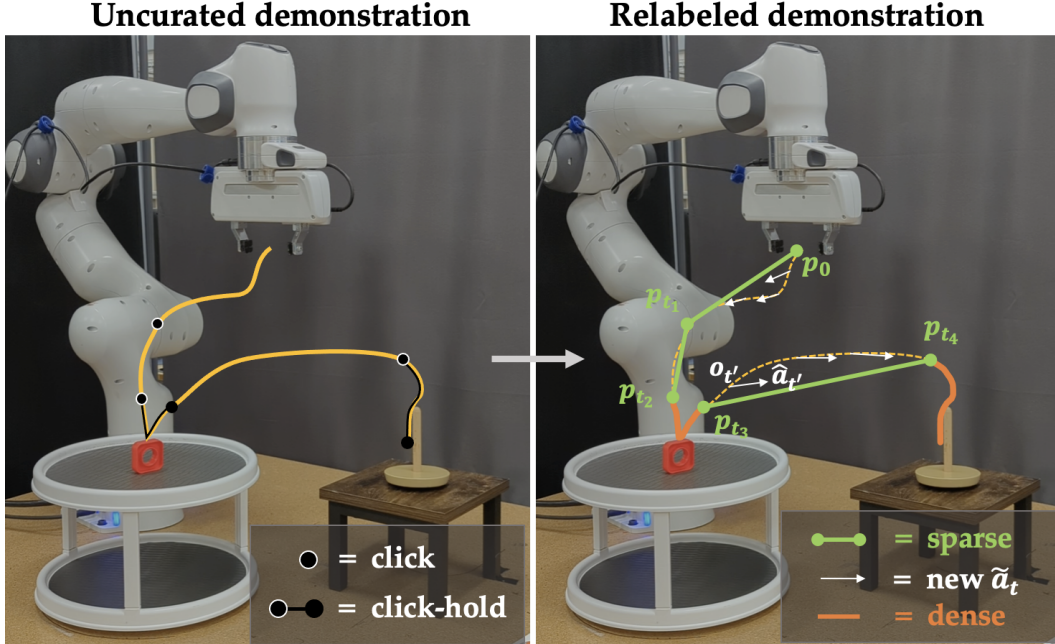


Figure 5: Mode labeling example for peg-insertion task. For each demo a human labels binary click signals at each time step (labeled online or offline) to segment trajectories into arbitrary sequences of sparse waypoint phases and dense action phases. **Left:** Uncurated demo, with single clicks and sustained clicks shown. **Right:** Relabeled demo, with waypoint and dense segments overlaid in green and orange, respectively. We also relabel actions for the states in sparse segments with the optimal waypoint reaching action shown in white. For sparse segments, the waypoint head of HYDRA is trained to output the final waypoint at each state along the trajectory.

467 With the trajectories segmented into sparse and dense modes, we can extract the desired future  
 468 waypoint  $w_t$  for each  $o_t$ : if  $m_t = 0$  (sparse), the future waypoint is the next labeled “single click”  
 469 proprioceptive state  $w_t = p_{t'}$  where  $t' > t$  (for example, states  $o_t$  with  $t_1 \leq t < t_2$  in Fig. 5 will use  
 470  $w_t = p_{t_2}$ ). But if  $m_t = 1$  (dense), the waypoint is the next proprioceptive state  $w_t = p_{t+1}$ . Thus we  
 471 construct a dataset of  $\hat{D}$  of  $(o_t, a_t, w_t, m_t)$  tuples. Now the policy has full supervision to learn both  
 472 the action and waypoint as well as the mode of operation. In Algorithm 1, we outline this process of  
 473 turning a click-labeled dataset into per-step waypoints and mode labels.

---

**Algorithm 1** Labeling Modes

---

- 1: Given click-labeled dataset:  $D = \{(o_t, a_t, c_t) \dots\}$
  - 2:  $\hat{D} = \{\}$
  - 3: **for all**  $t$  **do**
  - 4:    $m_t = c_t \ \& \ (c_{t-1} \mid c_{t+1})$  ▷ Sustained click for dense
  - 5:   *// Mark single click as waypoint*
  - 6:    $\text{isolated} = \neg c_{t-1} \ \& \ c_t \ \& \ \neg c_{t+1}$
  - 7:   *// Mark start of dense period as waypoint*
  - 8:    $\text{start\_dense} = \neg c_{t-1} \ \& \ m_t$
  - 9:   **if**  $\text{isolated}$  **or**  $\text{start\_dense}$  **then**
  - 10:      $w_{t_p:t-1} = p_t$  ▷ Set previous waypoints
  - 11:      $t_p = t$  ▷ start of next sparse phase
  - 12:   **else if**  $m_t = 1$  **then**
  - 13:     *// During dense mode the next state is a waypoint*
  - 14:      $w_t = p_{t+1}$
  - 15:      $t_p = t$
  - 16:   Add  $(o_t, a_t, w_t, m_t)$  to  $\hat{D}$
-

474 **B.2 Waypoint Controller**

475 For all experiments in the main text, we use a linear controller  $T_{\text{linear}}$  for reaching waypoints online.  
476 This means that when HYDRA predicts a waypoint period ( $\tilde{m}_t = 0$ ), it will servo closed loop until  
477 it reaches the predicted  $\tilde{w}_t$  or times out after  $N$  seconds. In all of our experiments, the waypoint  
478 follower times out after  $N = 5$  seconds if it has not reached the waypoint.

479 For this closed loop servoing during test time, the policy will still be *called*, but its outputs will  
480 be ignored. This is important for recurrent models specifically (e.g., Dense Net), since the hidden  
481 state for the policy should be updated similarly to how it was trained (on all states, even during  
482 the sparse period). While this mitigates the changes in the hidden state, this might still induce a  
483 different hidden state than was produced offline, since the human policy followed a non-optimal  
484 path to reach waypoint  $w$  from state  $s_t$ , as compared to the optimal online trajectory generated by  
485  $T$ . For example, if the demonstrator follows an arc-like trajectory to pick up a coffee pod and marks  
486 the waypoint right before picking up the coffee pod, then online the policy with  $T_{\text{linear}}$  will servo  
487 to that waypoint directly; the hidden state for these two paths will likely be different. This problem  
488 is difficult to observe in practice, and did not empirically show up in practice (as evidenced by the  
489 improved performance of our method compared to baselines).

490 In theory, one could bypass this issue by “skipping” the hidden state of the policy over entire sparse  
491 segments during training. Then during test time, if the policy outputs  $\tilde{m}_t = 0$ , the policy would not  
492 be called again until reaching the output  $w_t$ . However, this requires loading entire sparse segments  
493 and more in the training batches, which is computationally expensive and less simple than loading  
494 batches of fixed horizon as is commonly done. We leave a broader analysis of the hidden state  
495 problem for future work.

496 Additionally, we experimented with several controller gains and did not notice any effect on perfor-  
497 mance. Therefore we choose a fast controller to reach waypoints. These gains are constant for all  
498 experiments.

499 **B.3 Mode Labeling Sensitivity**

500 In our experiments, we noticed that mode labeling was quite robust to different labeling strategies  
501 provided that the labeling strategy satisfies the following guidelines.

502 **Waypoint Following Behaviors:** Waypoint following behaviors should be labeled for free-space  
503 motions in the environment, when the robot is “in transit” (e.g., reaching). As described in **Sec-**  
504 **tion 4.1**, a key consideration for mode labeling is making sure labels for sparse periods are compat-  
505 ible with the waypoint controller  $T$ . For example, if we are following a linear controller, waypoint  
506 segments should be reproducible with straight line segments from any start state along the waypoint  
507 segment. For a given  $(m_t, w_t, s_t)$ , then if  $m_t = 0$ , we should be able to reach waypoint  $w_t$  from  $s_t$   
508 with  $T$  (i.e. without timing out). As mentioned in the main text, if  $T$  includes collision avoidance as  
509 part of the controller, then we no longer have any requirements on waypoint following behaviors.

510 **Dense Object Interaction:** Dense periods should include (but is not limited to) all object interac-  
511 tions in the scene where “collision” with the scene is necessary (e.g., grasping a coffee pod, inserting  
512 the coffee pod into the coffee machine, picking up toast with a spatula). Humans excel at identify-  
513 ing these types of interactions, so these segments are quite easy to label. The exact amount of time  
514 “padded” onto these dense periods did not seem to affect learning in our experiments. Note that if  
515 each entire demo is treated as a dense period, our algorithm reduces to BC.

516 **Labeling Strategy Consistency:** The final consideration is for the consistency of the mode labeling  
517 strategy *between* different demonstrations. Variation in the exact boundaries / choices for waypoints  
518 and dense segments is inevitable with human labeling. While the effects of certain types of variation  
519 can be quite difficult to quantify in general, we believe that is important to minimize this variation  
520 without adding additional burden on the user. In our experiments, for each task and dataset, we  
521 have only one user provide the mode labels, according to a single strategy. For example, in the  
522 *NutAssemblySquare* task, where the goal is to insert a square nut onto a peg, a user might define the  
523 following strategy:

- 524 1. Reach waypoint above the square nut (sparse)
- 525 2. Go down, grasp, pick up (dense)
- 526 3. Move the nut up (sparse)
- 527 4. Move the nut above the insertion point (sparse)
- 528 5. precisely insert the nut on the peg (dense)

529 In general our method is quite robust to variations within a single mode labeling strategy (for a  
 530 single labeler), and we do no additional post-processing on mode labels or waypoints in any of our  
 531 experiments.

## 532 B.4 Training on Mode Labels

533 With labeled modes and waypoints, HYDRA learns to predict the mode, the waypoint, and the low-  
 534 level action at every time step according to the loss in Eqn. 4. However, due to training a higher  
 535 dimensional action space (e.g. for robot poses:  $|\mathcal{A}| = 7 + 7 + 1$ ) with a supervised objective, over-  
 536 fitting can be a key concern during training. For all vision-based experiments, we perform random  
 537 cropping to 90% the image size. However, there are several interesting mode-specific augmentations  
 538 that can be done using mode labels and waypoints to mitigate this problem:

539 **Mode Smoothing:** While the simple binary cross entropy mode loss in Eqn. 3 suffices for learning  
 540 to predict modes, sometimes the hard boundary between segments can lead to mode oscillation or  
 541 cycling when evaluating at test time. For example, model might predict a dense mode, then predict  
 542 a sparse mode at the next step that brings it back to the previous state, and repeat. In these cases  
 543 (which are rare in practice) it can be beneficial to *smooth* the mode labels to extract continuous  
 544 probabilities for the mode label at each step:  $p(\tau_m) = \text{convolve}(\tau_m, [\frac{1}{n}, \dots, \frac{1}{n}])$ , where  $n$  is the kernel  
 545 size. This yields the following loss:

$$\mathcal{L}_m(\theta) = -\mathbb{E}_{(o,a,w,m) \in \mathcal{D}} \left[ p(m) \log \pi_{\theta}^M(m = 1|o) + (1 - p(m)) \log \pi_{\theta}^M(m = 0|o) \right] \quad (5)$$

546 With this smoothing of the mode labels, we are effectively removing the hard boundary between  
 547 sparse and dense periods, which can help generalization for the mode prediction head of HYDRA  
 548 at test time.

549 **Waypoint Period Augmentation:** It is common in the literature to add small amounts of proprio-  
 550 ceptive state noise (increasing state diversity) to demonstrations. However, during object interaction  
 551 (i.e. dense periods), this noise can make policy learning more difficult since minor variations in  
 552 the state can have large changes in the action space. However, with knowledge of sparse and dense  
 553 modes in HYDRA, we could add diverse state augmentations to the proprioceptive state during only  
 554 the sparse periods. This waypoint period augmentation can help reduce overfitting in SparseNet,  
 555 since we will learn to reach the same waypoint (action) from many different robot poses (state).

556 Both mode smoothing and waypoint augmentation, while not utilized in our experiments, illustrate  
 557 the potential for new augmentation strategies that arise with access to mode labels.

## 558 C Model Architectures & Training

559 To train HYDRA, we use a similar procedure as in prior work [19, 14]. For each input of shape  
 560  $D_1 \times \dots \times D_N$ , we load sequential batches of size  $B \times H \times D_1 \times \dots \times D_N$ , where  $H$  is the horizon length.  
 561 Next we outline the network design for HYDRA, and hyperparameters used in each environment.

### 562 C.1 Network Design

563 As described in Section 4, HYDRA consists of SparseNet, which predicts the waypoint trajectory  
 564  $\tau_w$ , and DenseNet, which predicts the mode trajectory  $\tau_m$  and low level action trajectory  $\tau_a$ . Both  
 565 networks condition on the same input observation space (proprioceptive state trajectory  $\tau_{sp}$  and  
 566 environment state  $\tau_{se}$ ). For vision based experiments,  $s^p$  consists of both wrist mounted and external  
 567 camera observations. Each image is encoded via a ResNet18 architecture encoder (two encoders,  
 568  $E_{\theta}^{\text{ext}}, E_{\theta}^{\text{wrist}}$ , with separate parameters) which is trained end-to-end. Next, the image encodings are  
 569 concatenated along with the proprioceptive trajectory  $\tau_{sp}$ .

Environment	Method	# Demos	$B$	$H$	lr	$\gamma$	$\beta_m$	$ i $	$ D $	$ S $	$ \pi_\theta^A $	$ \pi_\theta^M $	GMM
NutAssemblySquare	BC	200	256	-	1e-4	-	-	-	400	-	-	-	0
	BC-RNN	200	256	10	1e-4	-	-	-	400	-	-	-	0
	HYDRA	200	256	10	1e-4	0.5	0.01	-	400	200	200	200	0
ToolHang	BC	200	256	-	1e-4	-	-	-	400	-	-	-	5
	BC-RNN	200	256	10	1e-4	-	-	-	1000	-	-	-	5
	HYDRA	200	256	20	1e-4	0.5	0.1	-	1000	400	400	400	0
KitchenEnv	BC-RNN	100	16	10	1e-4	-	-	64	1000	-	-	-	5
	HYDRA	100	16	10	1e-4	0.5	0.01	64	1000	400	400	400	5
PegInsertion	BC-RNN	75	8	10	1e-4	-	-	64	1000	-	-	-	0
	HYDRA	75	8	10	1e-4	0.5	0.01	64	1000	1000	1000	1000	0
MakeCoffee	BC-RNN	100	8	10	1e-4	-	-	64	1000	-	-	-	0
	HYDRA	100	8	10	1e-4	0.5	0.01	64	1000	1000	1000	1000	0
MakeToast	BC-RNN	80	8	10	1e-4	-	-	64	1000	-	-	-	0
	HYDRA	80	8	10	1e-4	0.5	0.01	64	1000	1000	1000	1000	0

Table 1: Hyperparameters for each environment, from left to right:  $B$  is batch size,  $H$  is the horizon length for training, lr is the learning rate,  $\gamma$  is the per time step weighting of the current mode,  $\beta_m$  is the weighting of the mode loss,  $|i|$  is the image encoding size (for each image),  $|D|$  is the hidden-size for recurrent dense networks (DenseNet, BC-RNN) or the MLP width (BC),  $|S|$  is the width of the SparseNet MLP (3 layers),  $|\pi_\theta^A|$  is the width of the action head (2 layers),  $|\pi_\theta^M|$  is the width of the mode head (2 layers), and finally GMM is the number of Gaussian mixtures (or 0 if deterministic) used for the dense action space. The top 3 rows are sim environments, where the first two are state only. The bottom three rows are vision-based real-world experiments. Hyperparameters stay mostly constant for HYDRA between experiments, with larger policy sizes for harder tasks. In almost all cases, BC-RNN, BC, and HYDRA share the same hyperparameters.

---

#### Algorithm 2 Training HYDRA

---

- 1: Given  $N$  (number of training steps)
  - 2: Given mode-labeled dataset:  $\hat{D} = \{(\tau_o, \tau_a, \tau_w, \tau_m) \dots\}$
  - 3: Networks  $E_\theta^{\text{ext}}, E_\theta^{\text{wrist}}, \pi_\theta^W, \pi_\theta^A, \pi_\theta^M$
  - 4: **for**  $i$  **in** range( $N$ ) **do**
  - 5:    $\tau_o, \tau_a, \tau_w, \tau_m \sim \hat{D}$  ▷ Load ( $B \times H \times \dots$ )
  - 6:    $\tau_i = E_\theta^{\text{wrist}}(\tau_o) \oplus E_\theta^{\text{ext}}(\tau_o) \oplus \tau_{sp}$  ▷ Encode
  - 7:    $\tau_w = \pi_\theta^W(\tau_i)$  ▷ waypoint (SparseNet)
  - 8:    $\tau_m = \pi_\theta^M(\tau_e)$  ▷ mode (DenseNet)
  - 9:    $\tau_a = \pi_\theta^A(\tau_e)$  ▷ action (DenseNet)
  - 10:   Compute  $\mathcal{L}(\theta)$  in Eqn. 4 and update  $\theta$
- 

## 570 C.2 Model & Training Details

571 Visual encoders use a ResNet-18 architecture trained end-to-end on both external images and end-  
572 effector images. We train all methods for 500k training steps over 3 random seeds, and like prior  
573 work we report the average over the best performing checkpoints per run [19]. We found that BC  
574 policy performance fluctuates significantly even for neighboring checkpoints. However, unlike prior  
575 work we use a *fixed* evaluation set of 50 episodes in simulation to choose the best checkpoint. This  
576 reduces the likelihood of choosing the checkpoint that was evaluated on favorable environments  
577 (i.e., rejection sampling of harder environment initialization).

578 For all experiments, our method uses an RNN (LSTM) for Dense Net (predicting the mode and the  
579 dense action), and uses a separate MLP with the same inputs for the Sparse Net (predicting sparse  
580 waypoints), as shown in Fig. 1.

581 The input embedding is then passed into SparseNet (MLP) which outputs the waypoint as a robot  
582 pose (position and quaternion). DenseNet can be any sequential model (RNN, Transformer, etc) that  
583 produces some temporal embedding  $\tau_e$  (RNN in our case). This architecture is shown in Fig. 6, and  
584 the training cycle is shown in Algorithm 2.

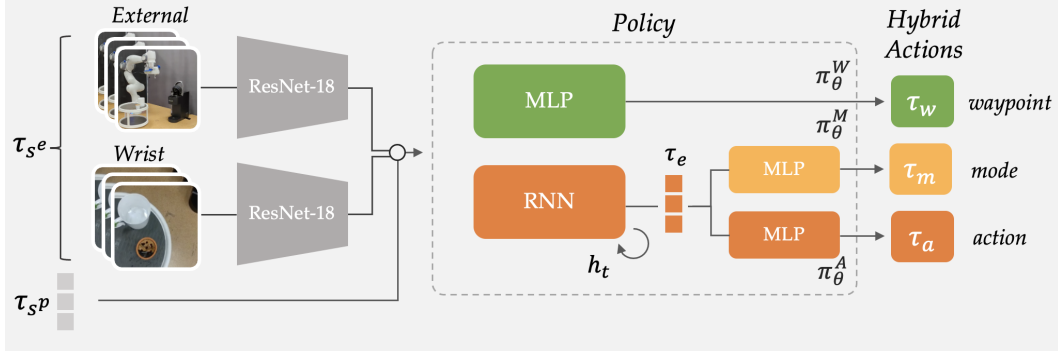


Figure 6: Specific instantiation of HYDRA for vision based experiments.

### 585 C.3 Evaluation Details

586 During evaluation (see Algorithm 3), the policy chooses the mode using  $\tilde{m}_t$ . If  $\tilde{m}_t = 0$ , the  
 587 model will servo in a closed-loop fashion to the predicted waypoint  $\tilde{w}_t$  (Line 7) using controller  
 588 T (Line 10). The policy is queried at every step to continually update the policy hidden state, but  
 589 importantly its outputs are ignored until we reach the waypoint to avoid action prediction errors.  
 (Line 4). If  $\tilde{m}_t = 1$ , the model will execute one step using the predicted dense action  $\tilde{a}_t$  (Line 14).

---

#### Algorithm 3 Test Time Execution

---

```

1: Given env,  $\pi(m, a, w|o)$ , initial state  $o_0$ , controller T
2:  $t = 0, w = \text{None}$ 
3: while not done do
4:    $\tilde{m}_t, \tilde{a}_t, \tilde{w}_t \sim \pi(\cdot|o_t)$  ▷ Sample policy
5:   // Check for new sparse mode
6:   if  $w$  is not set and  $\tilde{m}_t = 0$  then
7:      $w = \tilde{w}_t$  ▷ Set a new waypoint
8:   // Compute the waypoint-optimal action (sparse)
9:   if  $w$  is set but not reached and not timed-out then
10:     $\tilde{a}_t \leftarrow T(o_t, w)$  ▷ Compute waypoint-optimal action
11:   else
12:      $w = \text{None}$  ▷ Unset waypoint if reached
13:   // Step the environment
14:    $o_{t+1} = \text{env.step}(\tilde{a}_t)$ 
15:    $t = t + 1$ 

```

---

590

### 591 C.4 HYDRA Hyperparameters

592 The hyperparameters used in the main text for all six environments are shown in Table 1, for BC,  
 593 BC-RNN, and HYDRA. Hyperparameters stay mostly constant for HYDRA across all of the ex-  
 594 periments, with larger policy sizes for harder tasks. Additionally, in almost all cases, BC-RNN,  
 595 BC, and HYDRA share the same hyperparameters where possible. In the real world experiments,  
 596 hyperparameters are exactly the same both across methods and across environments.

## 597 D Additional Results & Analysis

598 In this section we show rollouts of our method and baselines, and then perform ablations of our  
 599 method and analyze the results, including mode labeling sensitivity, mode label learning from less  
 600 data, choices in action space design, different loss weightings, and robustness experiments. All  
 601 ablations are performed on the *NutAssemblySquare* task unless otherwise stated.

### 602 D.1 Rollouts for Real Environments

603 Fig. 7 shows example rollouts from the uncurated demonstration, the learned BC-RNN policy, and  
 604 HYDRA. Qualitatively, in the top row of Fig. 7 we see that HYDRA produces more consistent and

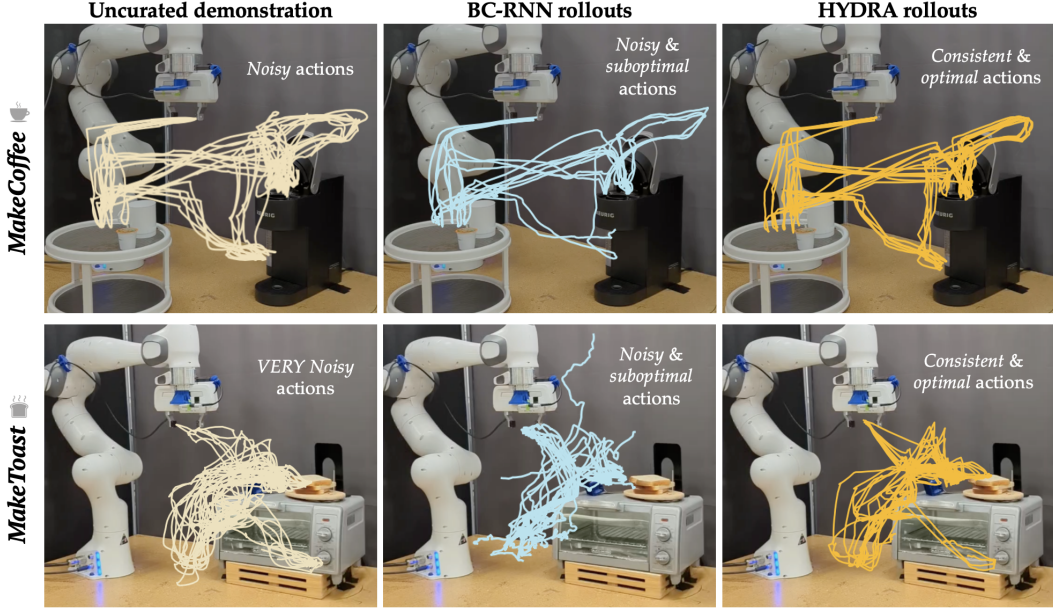


Figure 7: *MakeCoffee* (top) and *MakeToast* (bottom) rollouts, with the demos (left), HYDRA rollouts (middle), and BC-RNN rollouts (right). Our method produces more consistent and optimal actions compared to both BC-RNN and the demonstrations, and thus is able to stay within the narrow success “band” of the state distribution. BC-RNN has many sub-optimal behaviors, leading to less completed trajectories in middle column. The demonstrations for *MakeToast* are even noisier than those in *MakeCoffee*, leading to even more noticeable distribution shift for BC-RNN in the *MakeToast* task. In contrast, HYDRA *curates* the demonstrations in *MakeToast* using sparse and dense periods to follow more consistent paths, thus leading to higher success.

605 optimal trajectories at evaluation time that help the policy to stay within the narrow “band” of the  
 606 successful state distribution at test time, thus improving performance.

607 For the long horizon *MakeToast* task, the performance of HYDRA is much better than BC-RNN,  
 608 but lower overall than in *MakeCoffee*. We hypothesize that the difference between this task and  
 609 *MakeCoffee* is primarily in the consistency of demonstrated actions (see demonstration rollouts in  
 610 Fig. 7), with significant variation in the behaviors for nearby states especially during dense periods.  
 611 This leads to BC-RNN having highly noisy and sub-optimal actions, which manifest quite notice-  
 612 ably in Fig. 7. However, HYDRA yields much more consistent and optimal motions, reducing the  
 613 distribution-shift problem.

## 614 D.2 Mode Sensitivity

615 Next, we consider the sensitivity of HYDRA to mode labels, specifically in terms of the number of  
 616 labeled waypoints in each episode. In Table 2, we ablate the number of waypoints by introducing  $N$   
 617 intermediate waypoints in every sparse segment, for  $N = 1$  and  $N = 2$ . Since there are at least 3  
 618 sparse segments labeled in each demo in *NutAssemblySquare*, this corresponds to adding at least 3 or  
 619 6 more waypoints to each demonstration, respectively. We see that performance drops are relatively  
 620 minor in both cases, showing that HYDRA is robust to different waypoint choices. We hypothesize  
 621 that the reason for the minor performance change when adding more waypoints is that SparseNet  
 must learn a more complex waypoint space that is more multi-modal.

Base	Add-1	Add-2
90.0	86	80.0

Table 2: Success rates for HYDRA when artificially more waypoints are added to sparse periods. Adding intermediate waypoints to sparse segments has only a minor effect on performance despite the increase in complexity of the pose action space.

622

623 **D.3 Learning Mode Labels from Less Data**

624 Providing mode labels can be an additional overhead when training HYDRA. To reduce overhead,  
 625 we might want to learn the mode labels from a few labeled examples, and use this to relabel the rest  
 626 of the dataset. To show the promise of such an approach, we learn to predict the “click state” at  
 627 each time step (same as in Fig. 5) using a simple RNN architecture with the same parameters as the  
 628 model used for training. This model outputs two logits, one for the mode itself ( $m_t$ ), and one that  
 629 represents a switching criteria between segments ( $s_t$ ). This allows us to predict not only the sparse  
 630 or dense label, but also the waypoint label for each sparse segment. We additionally smooth both  
 631  $m_t$  and  $s_t$  as is commonly done in binary sequence prediction tasks. In Table 3, we demonstrate that  
 632 we can learn mode labels from 25% of the data with only a 10% drop in performance for the square  
 task, and even less of a drop when training on 50% or 75% of the data.

90%	75%	50%	25%
92	88	86	82

Table 3: Success rates for HYDRA for *NutAssemblySquare* when the mode labels are learned (predicting “click state” in Fig. 5).

633  
 634 With this preliminary evidence, we believe the sample efficiency of this mode learning procedure can  
 635 be improved by incorporating prior data from a wide range of tasks, potentially even using labeled  
 636 internet data. To address the multi-modality of mode labels that might occur when having multiple  
 637 people provide labels, future work might leverage few-shot or in-context learning approaches to  
 638 adapt to a particular *style* of mode labeling.

639 **D.4 Variations in the Action Space**

640 Why do we need the dense period at all? In Table 4, we compare HYDRA’s hybrid action space  
 641 to waypoint only ablations, both with and without the test-time controller  $T_{\text{linear}}$ . With  $T_{\text{linear}}$ , the  
 642 model outputs a waypoint and the robot reaches that waypoint using  $T_{\text{linear}}$  without querying the  
 643 policy (“open loop”), and without  $T_{\text{linear}}$ , the model outputs a new waypoint every step which gets  
 644 converted to action  $a$  using  $T_{\text{linear}}$  (“close loop”).

645 First we show results for WP-Next{N} in Table 4, where waypoints are the pose of the robot N steps  
 646 in the future at each state (hindsight relabeling). Second, we compare to WP-Mode, which uses  
 647 the same mode labels in HYDRA to get more intelligent future waypoints during sparse segments.  
 648 No pose-based models see any success, which we hypothesize is due to the mismatch between  
 649 the human action  $a$  and the online action  $T_{\text{linear}}(o, w)$ , which can lead to out of distribution states.  
 650 Even in the open loop case, the waypoint only models are unable to perform the task, with failures  
 651 involving imprecise behaviors during dense periods where exact velocities truly matter.

652 We additionally compare our method with and without the use of  $T_{\text{linear}}$  online (first column in  
 653 Table 4). We see that HYDRA greatly benefits from the online waypoint controller, since  $T_{\text{linear}}$   
 654 follows an optimal path while the policy-in-the-loop approach leaves room for compounding errors  
 655 in both the mode, action, and waypoint prediction. This once again illustrates that HYDRA yields  
 more consistent and optimal actions by employing a hybrid action abstraction.

	Ours	WP-Next1	WP-Next2	WP-Next5	WP-Mode
w/ T	90.0	0.0	0.0	2.0	0.0
w/o T	58.0	0.0	0.0	0.0	0.0

Table 4: Success rates for different action spaces. HYDRA uses a hybrid action space, while the the rest use a pose-based action space. Top row: waypoints are reached using  $T_{\text{linear}}$  before calling the policy again (“open” loop). Bottom row: waypoint actions are computed at every step and instead of reaching the action, the policy will convert a waypoint  $w$  to dense action  $a$  using  $T_{\text{linear}}$  (“closed” loop). WP-Next{N} uses the proprioceptive state N steps in the future as the waypoint for each state. WP-Mode uses the same mode labels as in HYDRA to get the waypoints, but does not implement a hybrid action space. None of the pose-based action spaces get reasonable performance, showing the importance of both dense actions and waypoint phases.

656  
 657 **D.5 Ablating Mode Weighting ( $\gamma$ )**

658 We also show the effect of different values of  $\gamma$ , the weight of the current mode loss. If for a given  
 659 step in training mode  $m_t = 0$  (sparse), then we weight the sparse waypoint loss for  $w_t$  with  $1 - \gamma$  and

660 the dense action loss for  $a_t$  with  $\gamma$ . Lower  $\gamma$  thus corresponds to fitting the current mode action loss  
 661 more than the other mode’s loss. Therefore,  $\gamma$  also controls the contribution of the relabeled actions  
 662 during sparse periods to the overall objective in Eq. (2). We use  $\gamma = 0.5$  in most experiments,  
 663 meaning both action (waypoint and dense action) losses are weighted equally during training. We  
 664 provide a sweep over  $\gamma$  in Table 5 for *NutAssemblySquare* and *ToolHang*, and we see that choosing  
 665  $\gamma$  only has a minor effect. Nonetheless,  $\gamma = 0.5$  is consistently the best. This illustrates that (1)  
 666 HYDRA is fairly robust to  $\gamma$ , (2) learning relabeled dense actions during sparse periods and sparse  
 667 actions during dense periods is beneficial to performance – this supports the claim in Section 4.1  
 668 that training on relabeled dense actions outperforms uncurated dense actions and

	$\gamma = 0.1$	$\gamma = 0.2$	$\gamma = 0.4$	$\gamma = 0.5$
Square	80.0	84.0	88.0	90.0
ToolHang	60.0	62.0	58.0	64.0

Table 5: Success rates for different values of  $\gamma$  for both *NutAssemblySquare* and *ToolHang*. For both *NutAssemblySquare* and *ToolHang*,  $\gamma$  does not have a large effect. We saw even less of a change for vision based experiments. Thus for real world experiments, we fix  $\gamma = 0.5$  (no mode-specific weighting).

## 669 D.6 Transformer-based architecture

670 In Table 6 we show the performance of a purely transformer-based BC implementation on the *KitchenEnv*  
 671 task. We see in this long horizon task that BC-RNN notably outperforms BC-Transformer in  
 672 this single-task imitation learning setting, and we found similar drops in performance for the state-  
 673 based simulation experiments. Thus, we did not include BC-Transformer as a baseline in our real  
 674 world experiments. We note that VIOLA, which uses a similar underlying transformer but with a  
 675 object-centric input representation, performs notably better on *KitchenEnv* than BC-Transformer.

	BC-RNN	BC-Transformer	VIOLA	HYDRA
Square	84	78.0	–	90.0
Kitchen	52.0	24.0	78.0	87.0

Table 6: Success rates for different values of BC architectures on *NutAssemblySquare* (state-based) and *KitchenEnv* (vision-based). For *NutAssemblySquare*, we see that using BC-Transformer minorly reduces performance. In *KitchenEnv*, we see a larger performance drop for BC-Transformer compared to BC-RNN. VIOLA proves a superior transformer based architecture compared to simple BC-Transformer for *KitchenEnv*. In all cases, HYDRA beats both RNN and Transformer-based baselines. All models share the same visual encoder structure and action spaces as described in Table 1.

## 676 D.7 Robustness of HYDRA to system noise

677 In Section 3 we noted the fundamental trade-off between consistent actions and state diversity. HY-  
 678 DRA breaks this tradeoff by relabeling actions in offline data, encouraging action consistency with-  
 679 out reducing the state coverage of the data. To show that HYDRA still benefits from the state  
 680 diversity in human data, in Table 7 we analyze the effect of system noise on HYDRA and BC. We  
 681 find that HYDRA only drops from 90% to 86% (4% drop) under the same system noise as used  
 682 with BC. This shows that not only does HYDRA capture the state diversity in human data, but it is  
 683 able to be even more robust to distribution shift than BC. We attribute this boost in part to the use  
 684 of a closed loop waypoint controller, which consistently reaches the waypoint under system noise.  
 685 This also supports the claim made in Section 6 that the gap in performance between HYDRA and  
 686 baselines in real compared to simulation experiments can in part be attributed to the added system  
 687 noise found in the real world.

	Base	Noise=0.1	Noise=0.3
BC-RNN	84	76.0	60.0
HYDRA	90	92.0	86.0

Table 7: The effect of increasing system noise (columns left to right) on BC-RNN (top row) and HYDRA (bottom row) trained on human data for *NutAssemblySquare*. While BC-RNN drops 24% under the max system noise, HYDRA only drops 4%, illustrating the ability of HYDRA to capture state diversity and thus be robust to distribution shift.